J|A|C|S
ARTICLES
Published on Web 04/05/2006

Protein−Cofactor Interactions and EPR Parameters for the Q_H Quinone Binding Site of Quinol Oxidase. A Density Functional Study

Sylwia Kacprzak,[†] Martin Kaupp,*[,†] and Fraser MacMillan[‡]

Contribution from the Institut für Anorganische Chemie, Universität Würzburg, Am Hubland, D 97074 Würzburg, Germany, and Institut für Physikalische und Theoretische Chemie, J. W. Goethe Universität Frankfurt, D-60439 Frankfurt am Main, Germany

Received June 16, 2005; E-mail: kaupp@mail.uni-wuerzburg.de

Abstract: Recent multifrequency EPR studies of the "high-affinity" quinone binding site of quinol oxidase (Q_H site) have suggested a very asymmetric hydrogen-bonding environment for the semiquinone radical anion state. Single-sided hydrogen bonding to the O_1 carbonyl position was one of the proposals, which contrasts with some previous experimental indications. Here density functional calculations of the EPR parameters (*g*-tensors, ^{13}C, ^{1}H, and ^{17}O hyperfine tensors) for a wide variety of supermolecular model complexes have been used to provide insight into the detailed relations among structure, environment, and EPR parameters of ubisemiquinone radical anions. A single-sided binding model is not able to account for the experimentally observed low g_x component of the *g*-tensor or for the observed magnitude of the asymmetry of the ^{13}C carbonyl HFC tensors. Based on the detailed comparison between computation and experiment, a model with two hydrogen bonds to O_1 and one hydrogen bond to O_4 is suggested for the Q_H site, but a model with one more hydrogen bond on each side cannot be excluded. Several general conclusions on the interrelations between EPR parameters and hydrogen bond patterns of ubisemiquinones in proteins are provided.

1. Introduction

Quinone cofactors are found in a remarkable multitude of redox enzymes.[1] Most often, the quinones employed by nature are ubiquinones (Figure 1), but phylloquinones, plastoquinones, or menaquinones are also frequently found.

More than 50 distinct types of quinone (Q) binding sites associated with respiratory or photosynthetic electron-transfer processes are known, and it has been suggested that many more may be discovered.[2] The function of the quinone is often that of a mediator between one-electron and two-electron redox processes. While binding initially either the oxidized quinone or fully reduced quinol, the Q binding sites stabilize the intermediate semiquinone oxidation state in the form of the paramagnetic semiquinone radical anion $Q^{\bullet-}$. Via spatial confinement of the quinone, the cofactor−protein interactions in the binding site serve to control electron-transfer processes from other parts of the protein to the quinone and vice versa. The interactions with the protein environment alter the potentials of the various redox states, thereby controlling the specific redox function of the quinone in a given system.[1] The relevant interactions include (a) hydrogen bonds, mainly to the quinone/semiquinone carbonyl oxygen atoms, and (b) π-stacking, e.g., with tryptophan residues. To understand the function of quinone cofactors in biological redox processes, knowledge of the cofactor−protein interactions is thus essential. Notably, information for the different relevant redox states should ideally be available. While protein crystallography typically provides information only about the neutral quinone or quinol states (but see, e.g., ref 3), the paramagnetic semiquinone state is often most effectively studied by spectroscopic methods, in particular by EPR spectroscopy.[4−6] The structurally best characterized

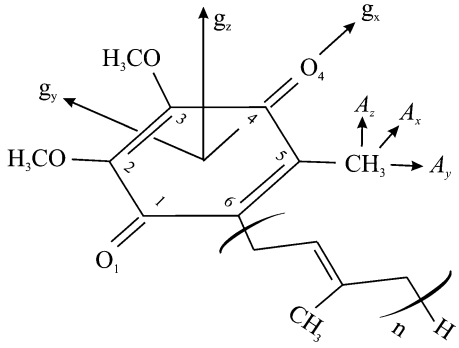

Figure 1. Structure of a general ubiquinone with atom labeling used throughout this work and with orientations of the semiquinone principal *g*-tensor and $^{1}H(CH_3)$ hyperfine tensor components.

[†] Universität Würzburg.
[‡] J. W. Goethe Universität Frankfurt.

(1) *The Chemistry of the Quinonoid Compounds, Pt. I and II*; Patai, S., Ed.; Wiley, Interscience: New York, 1974. *Function of Quinones in Energy Conserving Systems*; Trumpower, B. L., Ed.; Academic Press: New York, 1982. *Coenzyme Q: Biochemistry, Bioenergetics, and Clinical Applications of Ubiquinone*; Lenaz, G., Ed.; John Wiley & Sons: New York, 1985.
(2) Fisher, N.; Rich, P. R. *J. Mol. Biol.* **2000**, *296*, 1153−1162.
(3) Stowell, M. H. B.; McPhillips, T. M.; Rees, D. C.; Solitis, S. M.; Abresch, E.; Feher, G. *Science* **1997**, *276*, 812−816.
(4) Lubitz, W.; Feher, G. *Appl. Magn. Reson.* **1999**, *17*, 1−48.

quinone binding sites are certainly the Q_A and Q_B sites in photosynthetic reaction centers of purple bacteria.[3,7,8] The A_1 (Q_K) binding sites in photosystem I of higher organisms have also been studied in detail by crystallography[9] and spectroscopy.[10−12] Crystal structure information has recently been provided also for the Q_0 and Q_i sites of the respiratory bc_1 complexes[13] and for the menaquinone binding site of bacterial fumarate reductase.[14] At this point we will neglect the large number of characterized pyrolloquinolinequinones (PQQ) and flavins that may also be viewed as quinone redox cofactors.[15]

Often, however, less structural information is available, and what information there is may be incomplete or less direct. Then spectroscopy and computations may help to better understand the structures of the binding sites. Here we will use quantum chemical methods, combined with recently obtained multifrequency EPR data[16] and further available information, to elucidate the principal semiquinone binding mode in the "high-affinity" quinone binding site (Q_H site) in cytochrome bo_3 (bo_3 ubiquinol oxidase, QOX). The bo_3 QOX belongs to the family of terminal copper-heme oxidases of the respiratory chain.[17] In bacteria like *Escherichia coli*, the function of this enzyme is thus analogous to that of the mitochondrial cytochrome *c* oxidase,[18] which is the four-electron reduction of molecular oxygen to water in the cytoplasmic membrane. While the mechanism of dioxygen reduction is closely similar to that of cytochrome *c* oxidase (and the structural and functional elements involved are almost identical), in bo_3 QOX the electrons needed for reduction of O_2 do not derive from cytochrome *c* but from membrane-soluble ubiquinol-8. Ubiquinol oxidase is thought to have two ubiquinol/ubiquinone binding sites, a low-affinity Q_L and a high-affinity Q_H site.[19] The Q_H binding site has been suggested to act as a redox mediator between the two-electron oxidation of the quinol pool and the individual one-electron processes involved in reduction of oxygen at the heme-copper center.[19] It changes redox states between a quinone and a reduced semiquinone state. The X-ray structure of the bacterial bo_3 complex has been solved recently at 3.5 Å resolution,[20] but no quinones were bound in the crystal form. Functional studies combined with site-directed mutagenesis suggested a putative Q_H binding site, and four residues were postulated to be involved in direct binding to the cofactor (labels as for *Escherichia coli*): Asp75, Arg71, His98, and Gln101.[2] Clear information on individual interactions is, however, not available from these studies.

In this situation, EPR spectroscopy may provide additional important information, specifically on the semiquinone state.[4,5] Indeed, there have been several recent EPR and ENDOR studies of the Q_H semiquinone signal in the bacterial bo_3 QOX complex.[16,21−24] X-band EPR spectra provided evidence for the stabilization of a semiquinone radical anion in the Q_H site.[21] Numerical simulations of Q-band cw-EPR spectra[22] suggested that features seen in X-band spectra arise from hyperfine coupling to the protons of the ubisemiquinone methyl group in position 5 (Figure 1). Indications for exchangeable protons by ENDOR provided evidence for hydrogen bonds, either to one or to both semiquinone oxygens.[22] Based on ESEEM spectra, coupling of the unpaired electron density of the semiquinone radical anion to a nitrogen nucleus was identified, which was assigned as a peptide backbone nitrogen[24] (however an arginine[16] was not to be excluded), hydrogen-bonded to the 1-carbonyl oxygen atom (cf. Figure 1).

Using ubiquinone selectively ^{13}C-labeled at either the 1- or 4-carbonyl carbon position (Figure 1), Grimaldi et al. performed multifrequency EPR (X-, Q-, and W-band) measurements.[16] On one hand, they found an extremely low *g*-tensor anisotropy (low g_x value), which is usually attributed to strong hydrogen bonding.[25−29] On the other hand, a large asymmetry of the A_z components of the two ^{13}C carbonyl hyperfine tensors providing evidence for an appreciably asymmetrical spin density distribution was attributed to very asymmetrical hydrogen bonding. Single-sided hydrogen bonding to the 1-oxygen position was even suggested.[16] Previous detailed quantum chemical studies of the *g*-tensors of semiquinones in various environments showed, however, that single-sided hydrogen bonding to just one of the two carbonyl oxygen atoms will reduce the g_x component of the *g*-tensor much less than the same number of hydrogen bonds distributed over both oxygens, for reasons that

(5) Levanon, H.; Möbius, K. *Annu. Rev. Biophys. Biomol. Struct.* **1997**, *26*, 495−540.
(6) Prisner, T.; Rohrer, M.; MacMillan, F. *Annu. Rev. Phys. Chem.* **2001**, *52*, 279−313.
(7) (a) Blankenship, R. E. *Molecular Mechanisms of Photosynthesis*; Blackwell Science: Oxford, U.K., 2002. (b) Zouni, A.; Witt, H. T.; Kern, J.; Fromme, P.; Krauss, N.; Saenger, W.; Orth, P. *Nature* **2001**, *409*, 739−743.
(8) Ermler, U.; Fritzsch, G.; Buchanan, S. K.; Michel, H. *Structure* **1994**, *2*, 925−936.
(9) Jordan, P.; Fromme, P.; Witt, H. T.; Klukas, O.; Saenger, W.; Krauss, N. *Nature* **2001**, *411*, 909−917.
(10) MacMillan, F.; Hanley, J.; van der Weerd, L.; Knupling, M.; Un, S.; Rutherford, A. W. *Biochemistry* **1997**, *36*, 9297−9303.
(11) Zech, S. G.; van der Est, A. J.; Bittl, R. *Biochemistry* **1997**, *36*, 9774−9779.
(12) Zech, S. G.; Hofbauer, W.; Kamlowski, A.; Fromme, P.; Stehlik, D.; Lubitz, W.; Bittl, R. *J. Phys. Chem. B* **2000**, *104*, 9728−9739.
(13) (a) Iwata, S.; Lee, J. W.; Okada, K.; Lee, J. K.; Iwata, M.; Rasmussen, B.; Link, T. A.; Ramaswamy, S.; Jap, B. K. *Science* **1998**, *281*, 64−71. (b) Xia, D.; Yu, C. A.; Kim, H.; Xia, J. Z.; Kachurin, A. M.; Zhang, L.; Yu, L.; Deisenhofer, J. *Science* **1997**, *277*, 60−66. (c) Hunte, C.; Koepke, J.; Lange, C.; Rossmanith, T.; Michel, H. *Structure* **2000**, *8*, 669−684.
(14) (a) Iverson, T. M.; Luna-Chavez, C.; Cecchini, G.; Rees, D. C. *Science (Washington, D.C.)* **1999**, *284*, 1961−1966. (b) Li, R.; Bianchet, M. A.; Talalay, P.; Amzel, L. M. *Proc. Natl. Acad. Sci. U.S.A.* **1995**, *92*, 8846−8850.
(15) Xia, Z.-X.; Dai, W.-W.; He, Y.-N.; White, S. A.; Mathews, F. S.; Davidson, V. L. *Journal of Biological Inorganic Chemistry* **2003**, *8*, 843−854.
(16) Grimaldi, S.; Ostermann, T.; Weiden, N.; Mogi, T.; Miyoshi, H.; Ludwig, B.; Michel, H.; Prisner, T. F.; MacMillan, F. *Biochemistry* **2003**, *42*, 5632−5639.
(17) Garcia-Horsman, J. A.; Barquera, B.; Rumbley, J.; Ma, J.; Gennis, R. B. *J. Bacteriol.* **1994**, *176*, 5587−5600.
(18) (a) Kranz, R. G.; Gennis, R. B. *J. Biol. Chem.* **1983**, *258*, 10614−10621. (b) Puustinen, A.; Finel, M.; Haltia, T.; Gennis, R. B.; Wikstrom, M. *Biochemistry* **1991**, *30*, 3936−3942. (c) Puustinen, A.; Wikstrom, M. *Proc. Natl. Acad. Sci. U.S.A.* **1991**, *88*, 6122−6126. (d) Puustinen, A.; Morgan, J. E.; Verkhovskii, M.; Thomas, J. W.; Gennis, R. B.; Wikstrom, M. *Biochemistry* **1992**, *31*, 10363−10369.
(19) Sato-Watanabe, M.; Mogi, T.; Ogura, T.; Kitagawa, T.; Miyoshi, H.; Iwamura, H.; Anraku, Y. *J. Biol. Chem.* **1994**, *269*, 28908−28912.
(20) Abramson, J.; Riistama, S.; Larsson, G.; Jasaitis, A.; Svensson-Ek, M.; Laakkonen, L.; Puustinen, A.; Iwata, S.; Wikstrom, M. *Nat. Struct. Biol.* **2000**, *7*, 910−917.
(21) (a) Ingledew, W. J.; Ohnishi, T.; Salerno, J. C. *Eur. J. Biochem.* **1995**, *227*, 903−908. (b) Sato-Watanabe, M.; Itoh, S.; Mogi, T.; Matsuura, K.; Miyoshi, H.; Anraku, Y. *FEBS Lett.* **1995**, *374*, 265−269.
(22) Veselov, A. V.; Osborne, J. P.; Gennis, R. B.; Scholes, C. P. *Biochemistry* **2000**, *39*, 3169−3175.
(23) Hastings, S. F.; Heathcote, P.; Ingledew, W. J.; Rigby, S. E. *Eur. J. Biochem.* **2000**, *267*, 5638−5645.
(24) Grimaldi, S.; MacMillan, F.; Ostermann, T.; Ludwig, B.; Michel, H.; Prisner, T. *Biochemistry* **2001**, *40*, 1037−1043.
(25) (a) Zandstra, P. J. *J. Chem. Phys.* **1964**, *41*, 3655−3656. (b) Hales, B. J. *J. Am. Chem. Soc.* **1975**, *97*, 5993−5997. (c) *CRC handbook of EPR spectra from quinones and quinols*; Pedersen, J. A., Ed.; CRC Press: Boca Raton, FL, 1985. (d) Stone, A. J. *Proc. R. Soc. London, Ser. A* **1963**, *271*, 424−434. (e) Stone, A. J. *Mol. Phys.* **1963**, *6*, 509−515.
(26) Burghaus, O.; Plato, M.; Rohrer, M.; Möbius, K.; MacMillan, F.; Lubitz, W. *J. Phys. Chem.* **1993**, *97*, 7639−7647.
(27) Rohrer, M.; Plato, M.; MacMillan, F.; Grishin, Y.; Lubitz, W.; Möbius, K. *J. Magn. Reson.* **1995**, *116*, 59−66.
(28) Isaacson, R. A.; Lendzian, F.; Abresch, E. C.; Lubitz, W.; Feher, G. *Biophys. J.* **1995**, *69*, 311−322.
(29) Nimz, O.; Lendzian, F.; Boullais, C.; Lubitz, W. *Appl. Magn. Reson.* **1998**, *14*, 255−274.

we will review further below.[30] Therefore, very low *g*-anisotropies appear incompatible with single-sided hydrogen bonding. ENDOR data from plastoquinone-substituted samples were also interpreted in terms of a more symmetrical hydrogen-bonding framework.[23] To characterize the hydrogen bonding environment of the semiquinone radical anion in the Q_H site of bo_3 quinol oxidase in more detail, these somewhat contradictory findings require further investigation. Here we employ modern density functional methods to compute the *g*- and *A*-tensors of suitable hydrogen-bonded model complexes. Based on a detailed comparison between computed and experimental *g*-tensors and hyperfine tensors, we arrive at an improved binding model for the Q_H site that involves asymmetric but not single-sided hydrogen bonding. The relevance of the present study extends beyond the insight into the target system, quinol oxidase, and provides a systematic investigation of the effects of hydrogen bonding on EPR parameters of ubisemiquinone anions in proteins.

2. Computational Details

Structure Optimizations and Models. Previous experience in comparison with experiment and with more sophisticated computational approaches suggests that the effects of hydrogen bonds on the EPR parameters of semiquinone radical anions may be modeled well by density functional (DFT) calculations on relatively small supermolecular complexes. This holds for both *g*-tensors[30−34] and hyperfine tensors.[35,36] In the absence of more specific structural information, we have chosen to employ either water molecules or *N*-methyl-formamide (nmf), or both, as hydrogen-bond donors to the semiquinone. As the nature of the isoprenoid side chain of the ubisemiquinone radical anion (cf. Figure 1) has been found both experimentally and computationally to influence the *g*-tensor and most hyperfine parameters only negligibly,[26,27,37] it has been replaced by an ethyl group in our models (UQ-E$^{\bullet-}$). For the majority of models, all substituents were on the same side of the semiquinone ring in the starting structure, as found in the X-ray structure of $Q_A^{\bullet-}$.[3] However, in view of the low rotational barriers,[37] other conformations, such as those represented by models 2/1-c and 2/1-d, cannot be excluded. Most of the resulting model complexes are shown in Figure 2.

All structures have been fully optimized at the DFT level, using the gradient-corrected BP86 functional[38] and a DZVP Gaussian-type-orbital basis set.[39] SVP auxiliary basis sets[40] were used to fit the electron density (RI-DFT approximation). Unless stated otherwise, the calculations were performed with the TURBOMOLE program[41] (version 5.6). In some calculations, we have simulated roughly the electrostatic influence of *heme a*,[20] using a +2 point charge at positions relative to the semiquinone model 2/1-a 1HO-1HN-4HO (Figure 2b) that are compatible with the suggested binding site.[20] The possibility of a weak single hydrogen bond to O_4 has been evaluated by examining structures, again based on the 2/1-a 1HO-1HN-4HO model (Figure 2b), in which the hydrogen-bond distance to O_4 was increased in steps of 0.05 Å from the optimized 1.79 Å up to 2.34 Å. Using the same 2/1-a model, the potential effect of very strong hydrogen bonding was investigated by shortening all or only selected hydrogen bonds to 1.60 Å (Table S2 in the Supporting Information).

Four more specific supermolecular models from a previous computational study[32] have been included for comparison: models for ubisemiquinone anion radicals in both the $Q_A^{\bullet-}$ and $Q_B^{\bullet-}$ binding sites of bacterial reaction centers, one model for ubisemiquinone in frozen 2-propanol (with six 2-propanol molecules hydrogen-bonded to ubisemiquinone), and a model for phyllosemiquinone in the $A_1^{\bullet-}$ binding site of PS-I. The models in ref 32 were prepared based on crystal structure data for the intermolecular arrangement and on DFT-optimized fragments (with optimization of the positions of the H-bonded hydrogen atoms in bimolecular complexes[32]). We have initially used those structures directly for the EPR parameter calculations (note that the *g*-tensor results will nevertheless differ slightly from those in ref 32 due to a somewhat different *g*-tensor implementation). For the $Q_A^{\bullet-}$, $Q_B^{\bullet-}$, and $A_1^{\bullet-}$ binding-site models, we have additionally performed partial optimizations in which the heavy atoms of the H-bond donors have been kept at fixed positions, but the entire semiquinone and the H-bonded protons were free to move (see Table 2 below for details, as well as Figures 1−4 in ref 32). All these partial optimizations were performed with the Gaussian 03 program.[42] Both the initial Cartesian coordinates[32] and the reoptimized structures of all these more sophisticated models are compared in Table S3 in the Supporting Information.

***g*-Tensor Calculations.** The *g*-tensor calculations employed the second-order perturbation approach delineated in ref 43, which has been demonstrated to provide unprecedented accuracy in calculations of *g*-tensors for organic radicals (see also a recent review on *g*-tensor calculations for organic radicals[44]). Unlike most of our previous static calculations of semiquinones,[30−32] but analogous to recent dynamical studies of aqueous benzosemiquinone,[34] the Kohn−Sham orbitals were obtained with the TURBOMOLE program and involved the fitting of charge density but not of exchange-correlation potential. This provides about 5% larger Δg_x components of the *g*-shift tensors compared to previous extensive studies within the deMon program framework, where both density and potential were fitted.[30−32] In the latter case, we found RI-BP86/DZVP calculations to overestimate the most sensitive Δg_x tensor component systematically, and a scaling factor of 0.92 was found to provide the best agreement between supermolecular model calculations and experimental data in protic solution.[30] Given the larger Δg_x components obtained in the current procedure (also at the RI-BP86/DZVP level), a scaling factor of 0.88 is more appropriate[34] and will be used throughout this work. The unrestricted Kohn−Sham MO information from TURBOMOLE was transferred by appropriate interface routines to the MAG (magnetic resonance) property module of the in-house program ReSpect.[45] The one- and two-electron spin−orbit (SO) operators were treated by the accurate and efficient all-electron atomic

(30) Kaupp, M.; Remenyi, C.; Vaara, J.; Malkina, O. L.; Malkin, V. G. *J. Am. Chem. Soc.* **2002**, *124*, 2709−2722.
(31) Kaupp, M. *Biochemistry* **2002**, *41*, 2895−2900.
(32) Kacprzak, S.; Kaupp, M. *J. Phys. Chem. B* **2004**, *108*, 2464−2469.
(33) (a) Ciofini, I.; Reviakine, R.; Arbuznikov, A.; Kaupp, M. *Theor. Chem. Acc.* **2004**, *111*, 132−140. (b) Sinnecker, S.; Reijerse, E.; Neese, F.; Lubitz, W. *J. Am. Chem. Soc.* **2004**, *126*, 3280−3290.
(34) (a) Asher, J. R.; Doltsinis, N. L.; Kaupp, M. *J. Am. Chem. Soc.* **2004**, *126*, 9854−9861. (b) Asher, J. R.; Doltsinis, N. L.; Kaupp, M. *Magn. Reson. Chem.* **2005**, *43*, S237−S247.
(35) (a) O'Malley, P. J. *J. Phys. Chem. A* **1997**, *101*, 6334−6338. (b) O'Malley, P. J. *J. Phys. Chem. A* **1998**, *102*, 248−253. (c) O'Malley, P. J. *J. Am. Chem. Soc.* **1998**, *120*, 5093−5097. (d) Eriksson, L. A.; Himo, F.; Siegbahn, P. E. M.; Babcock, G. T. *J. Phys. Chem. A* **1997**, *101*, 9496−9504. (e) Himo, F.; Babcock, G. T.; Eriksson, L. A. *J. Phys. Chem. A* **1999**, *103*, 3745−3749. (f) Grafton, A. K.; Wheeler, R. A. *J. Phys. Chem. A* **1997**, *101*, 7154−7166. (g) Boesch, S. E.; Wheeler, R. A. *J. Phys. Chem. A* **1997**, *101*, 5799−5804. (h) Wise, K. E.; Grafton, A. K.; Wheeler, R. A. *J. Phys. Chem. A* **1997**, *101*, 1160−1165. (i) Nonella, M. *Photosynth. Res.* **1998**, *55*, 253−259. (j) Zhan, C.-G.; Chipman, D. M. *J. Phys. Chem. A* **1998**, *102*, 1230−1235.
(36) Nonella, M. *J. Phys. Chem. B* **1998**, *102*, 4217−4225.
(37) MacMillan, F.; Lendzian, F.; Lubitz, W. *Magn. Reson. Chem.* **1995**, *33*, 81−93.
(38) (a) Becke, A. D. *Phys. Rev. A* **1988**, *38*, 3098−3100. (b) Perdew, J. P.; Wang, Y. *Phys. Rev. B* **1986**, *33*, 8822−8824.
(39) Godbout, N.; Salahub, D. R.; Andzelm, J.; Wimmer, E. *Can. J. Chem.* **1992**, *70*, 560−571.
(40) Eichkorn, K.; Treutler, O.; Öhm, H.; Häser, M.; Ahlrichs, R. *Chem. Phys. Lett.* **1995**, *242*, 652−660.
(41) (a) Ahlrichs, R.; Bär, M.; Häser, M.; Horn, H.; Kölmel, C. *Chem. Phys. Lett.* **1989**, *162*, 165−169. (b) Ahlrichs, R.; von Arnim, M. In *Methods and Techniques in Computational Chemistry*; Clementi, E., Corongiu, G., Eds.; Club Europeen MOTECC: 1995; Chapter 13, p 509.
(42) Frisch, M. J. et al. *Gaussian 03*; Gaussian, Inc.: Wallingford CT, 2004.
(43) (a) Malkina, O. L.; Vaara, J.; Schimmelpfennig, B.; Munzarova, M.; Malkin, V. G.; Kaupp, M. *J. Am. Chem. Soc.* **2000**, *122*, 9206−9218. (b) Kaupp, M.; Reviakine, R.; Malkina, O. L.; Arbuznikov, A.; Schimmelpfennig, B.; Malkin, V. G. *J. Comput. Chem.* **2002**, *23*, 794−803.
(44) Kaupp, M. EPR Spectroscopy of Free Radicals in Solids. Trends in Methods and Applications. In *Progress in Theoretical Chemistry and Physics*; Lund, A., Shiotani, M., Eds.; Kluwer: Dordrecht, 2003; Vol. 10, pp 267−302.

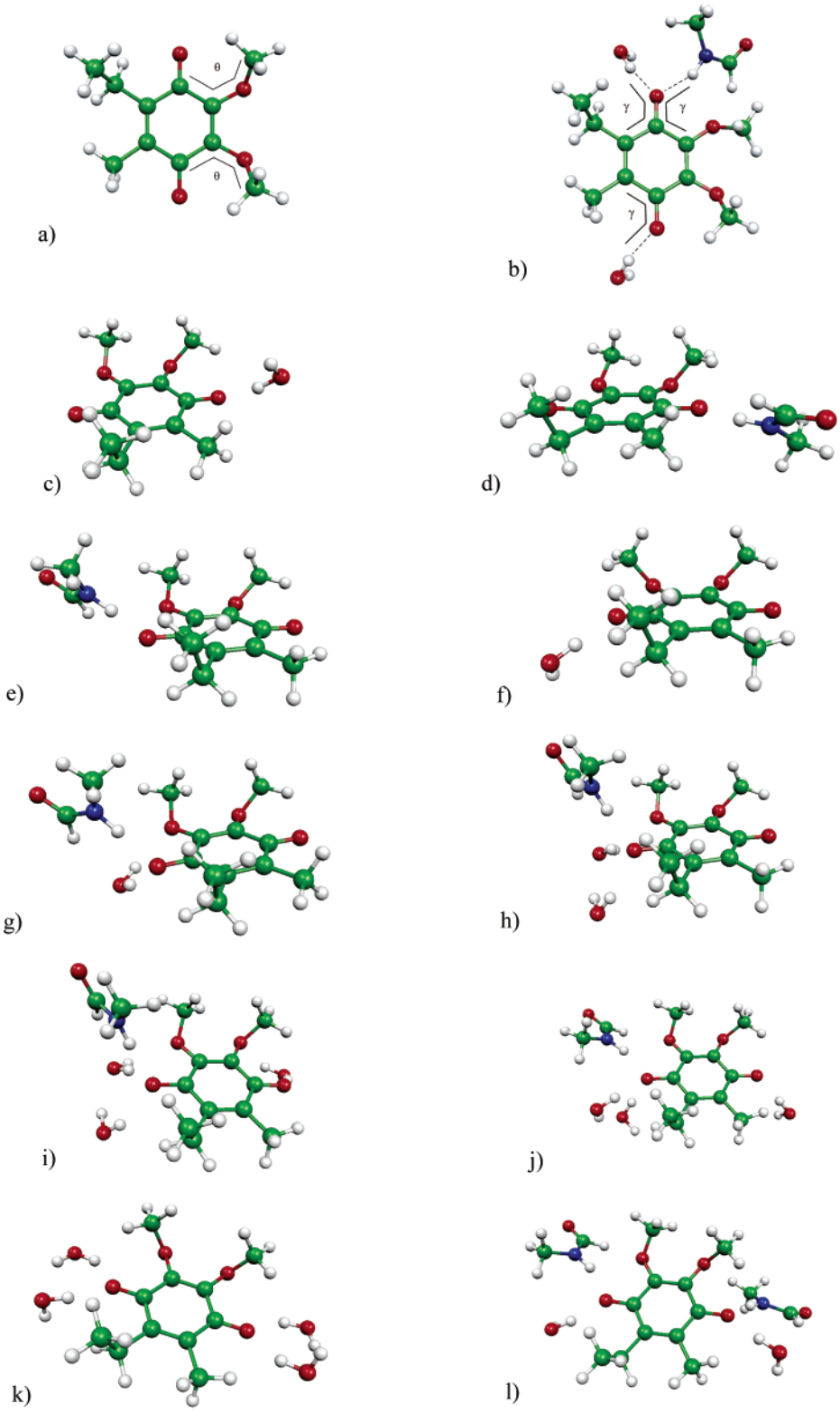

Figure 2. Optimized structures of supermolecular model complexes studied. Numbers *n*/*m* indicate the number of hydrogen bonds to O_1 and O_4, respectively, and the labels HO and HN indicate a water molecule and an *N*-methylformamide molecule, respectively: (a) naked UQ-E, 0/0 model; definition of methoxy dihedral angles θ_1 and θ_2; (b) 2/1-a model 1HO-1HN-4HO; definition of hydrogen-bonding dihedral angle γ; (c) 0/1 model 4HO; (d) 0/1 model 4HN; (e) 1/0 model 1HN; (f) 1/0 model 1HO; (g) 2/0 model 1HO-1HN; (h) 3/0 model 1HO-1HO-1HN; (i) 3/1-a model 1HO-1HO-1HN-4HO (this model involves bridging hydrogen bonds to the methoxy oxygen atoms); (j) 3/1-b model 1HO-1HO-1HN-4HO; (k) 2/2-a model 1HO-1HO-4HO-4HO; (l) 2/2-b model 1HO-1HN-4HO-4HN.

meanfield approximation (AMFI).[46] The common gauge origin for the external magnetic vector potential was chosen to be at the midpoint between the two carbonyl oxygen atoms. This is expected to be close to the center of spin density. In our calculations, the *g*-tensor is defined as $\mathbf{g} = g_e(\mathbf{1}) + \mathbf{\Delta g}$, where $g_e = 2.002\,319$. We present and discuss *g*-shift components (Δg_i) defined as corrections to the free electron

Table 1. Hydrogen Bond Lengths, Hydrogen-Bond Dihedral Angles,[a] and Methoxy-Group Out-of-Plane Dihedral Angles[a]

	d(H···O) in Å; absolute dihedral angle γ in deg						dihedral angles θ of methoxy groups
model	O_1···HO; γ	O_1···HO; γ	O_1···HN; γ	O_4···HO; γ	O_4···HN; γ	O_4···HO; γ	θ_1; θ_2
0/1 4HO				1.76; 51			132; −58
0/1 4HN					1.75; 2		137; −61
1/0 1HN			1.76; 18				138; −58
1/0 1HO	1.76; 21						62; −57
2/0 1HO-1HN	1.79; 58		1.82; 22				139; −58
3/0 1HO-1HO-1HN	1.81; 30	2.08; 63	1.89; 62				130; −55
1/1 1HN-4HN			1.81; 3			1.78; 27	136; −59
3/1-a 1HO-1HO-1HN-4HO	1.80; 29	2.11; 61	1.92; 61	1.88; 40			135; −64
3/1-b 1HO-1HO-1HN-4HO	1.82; 78	2.06; 20	1.95; 11	1.81; 43			140; −59
2/2-a 1HO-1HO-4HO-4HO	1.76; 3	2.10; 24		1.75; 18		2.11; 22	68; −69
2/2-b 1HO-1HO-4HO-4HO	1.75; 0	2.12; 27		1.77; 20		2.11; 55	−82; 63
2/1-a 1HO-1HN-4HO	1.78; 17		1.89; 3	1.79; 32			132; −57
2/1-b 1HO-1HN-4HO	1.78; 17		1.91; 9	1.80; 33			110; −51
2/1-c 1HO-1HN-4HO	1.78; 13		1.90; 8	1.80; 31			106; 60
2/1-d 1HO-1HN-4HO	1.76; 32		1.89; 25	1.79; 38			−92; −60
2/1 1HN-1HN-4HN			1.85; 16		1.80; 27		137; −59
			1.93; 2				
1/2 1HO-4HO-4HN	1.80; 18			1.79; 14	1.88;36		58; −66
3/2 1HO-1HO-1HN-4HO-4HN	1.84; 75	2.08; 25	1.97; 11	1.81; 19	1.90;41		144; −66
2/2 1HO-1HN-4HO-4HN	1.80; 9		1.91; 1	1.80; 24	1.87; 42		142; −65
2/3 1HO-1HN-4HO-4HO-4HN	1.81; 6		1.92; 1	1.88; 78	1.93; 37	1.87; 40	146; −69

[a] Cf. Figure 2a,b for definition of dihedral angles.

value in ppm (that is, in units of 10^{-6}). Our approach includes not only the dominant second-order spin−orbit/orbital-Zeeman cross terms but also the relativistic mass correction (RMC) and the one-electron part of the spin−orbit gauge correction (GC) terms.[43]

Hyperfine Tensor Calculations. All hyperfine coupling parameters were computed in the usual nonrelativistic first-order approach, using the MAG-ReSpect[45] code based on unrestricted Kohn−Sham wave functions obtained with the TURBOMOLE[41] program. It is well-known that gradient-corrected functionals such as BP86 underestimate the spin polarization in π-radicals and thus provide less accurate hyperfine couplings. In contrast to the optimizations and g-tensor calculations the hyperfine calculations used therefore the B3LYP[47] hybrid functional (in nonlocal implementation, cf. ref 48 for a discussion) in combination with the somewhat larger EPR-II[49] basis set (which was specifically designed for hyperfine calculations). Further test calculations with other functionals, and also with the more extended EPR-III basis, provided only relatively minor modifications of the results.

3. Results and Discussion

Structures of Model Complexes. Figure 2 shows optimized structures for the chosen model systems. In most cases, the hydrogen bonds occur not too far outside the plane of the semiquinone, with dihedral angles γ typically below 30°−40° (Table 1; cf. definition of γ in Figure 2b).

Somewhat larger out-of-plane angles occur particularly for models with more than two hydrogen bonds to an oxygen or when the overall hydrogen-bond situation becomes crowded for other reasons. Some ENDOR data suggest strong out-of-plane hydrogen bonding in the Q_H site,[23] and it is possible that our structures do not capture this completely. However, still more pronounced out-of-plane hydrogen bonds would lead to (a) slightly larger and not lower Δg_x values (see below)[30] and (b) probably only minor effects on $^{13}C(CO)$ and $^{1}H(CH_3)$ hyperfine tensors. In the absence of more detailed structural information, we regard the chosen models as reasonable. Notably, we have computed EPR parameters for (i) the naked UQ-$E^{\bullet-}$ radical anion, (ii) systems with single-sided hydrogen bonding either to O_1 or to O_4, and (iii) symmetric or asymmetric double-sided hydrogen bonding. We have found several minimum structures for our most promising 2/1 1HO-1HN-4HO model. They are all within 3 kJ mol^{-1} of each other and give relatively similar EPR parameters (see below). It is clear that a more complete treatment would have to include extensive molecular dynamics,[34] but this is outside the scope of the present study.

In the presence of only one contact to a carbonyl oxygen, the computed hydrogen bond lengths (Table 1) are similar to those in benzosemiquinone complexes. As soon as we have more than one hydrogen bond, some of the contacts become appreciably longer than those found for the parent system,[30] in particular when we force three hydrogen bonds to the same oxygen atom. This is due to the steric influence of the substituents in ubisemiquinones, which is also responsible for the out-of-plane character of the hydrogen bonds. In several of the 2/2, 3/2, 3/1, or 3/0 models, one of the hydrogen bonds to a given oxygen is noticeably longer (>2.0 Å) than the other(s), provided more than one water molecule is involved at this site (Table 1). In previous calculations on a UQ-$M^{\bullet-}$ model (dimethoxy-dimethylsemiquinone) with four (or six) water or alcohol molecules, we did not observe this behavior.[30] Closer analysis indicates that the hydrogen bond preferences are strongly coupled to the conformations of the methoxy substituents (dihedral angle θ in Table 1; see definition in Figure 2a), and the previous calculations did not represent optimum conformations (computed energies for the present structures are

(45) Malkin, V. G.; Malkina, O. L.; Reviakine, R.; Arbuznikov, A. V.; Kaupp, M.; Schimmelpfennig, B.; Malkin, I.; Helgaker, T.; Ruud, K. *MAG-ReSpect*, version 1.1; 2003.
(46) (a) Hess, B. A.; Marian, C. M.; Wahlgren, U.; Gropen, O. *Chem. Phys. Lett.* **1996**, *251*, 365−371. (b) Schimmelpfennig, B. *Atomic Spin−Orbit Mean-Field Integral Program*; Stockholms Universitet: Stockholm, Sweden, 1996.
(47) (a) Becke, A. D. *J. Chem. Phys.* **1993**, *98*, 5648−5652. (b) Lee, C.; Yang, W.; Parr, R. G. *Phys. Rev. B* **1988**, *37*, 785−789. (c) Miehlich, B.; Savin, A.; Stoll, H.; Preuss, H. *Chem. Phys. Lett.* **1989**, *157*, 200−206.
(48) (a) Arbuznikov, A. V.; Kaupp, M. *Chem. Phys. Lett.* **2004**, *391*, 16−21. (b) Arbuznikov, A. V.; Kaupp, M. *Chem. Phys. Lett.* **2004**, *386*, 8−16.
(49) Barone, V. In *Recent Advances in Density Functional Methods*; Chong, D. P., Eds.; World Scientific Publishing Co.: Singapore, 1996; Part I.

somewhat lower). In the majority of cases, where both methoxy substituents are on the same side of the ring, θ_1 is near 130°−140° and θ_2, near −55° to −60° (see ref 36 for other DFT calculations on models without hydrogen bonding). This corresponds to both methoxy groups being tilted in the direction of the same carbonyl group (Figure 2). There are a few exceptions, e.g., for the 1/0 HO model (Figure 2f) or for both 2/2 models with four water molecules (the 2/2-a model is shown in Figure 2k), where an opposite orientation is preferred. Obviously, our static optimizations, although carried out from many different starting points, cannot guarantee that we have in all cases found the global minimum. We are currently carrying out ab initio molecular dynamics simulations for aqueous ubisemiquinone[50] (cf. ref 34 for related work on benzosemiquinone) to obtain further insight into the conformational preferences.

The experimental evidence for the QOX Q_H site does not seem to suggest hydrogen bonding to the methoxy substituents[51] (in contrast to protic solution[30]). Therefore we prefer in Table 1 structures in which the water molecules do not bridge between carbonyl oxygen and methoxy groups. The 3/1-a structure is a notable exception. A wide range of H-bond out-of-plane angles is found for the more sophisticated $Q_A^{\bullet-}$, $Q_B^{\bullet-}$, and $A_1^{\bullet-}$ models.[32] The largest (experimental) γ value is 87° for $Q_B^{\bullet-}$, and the smallest, 13° for $A_1^{\bullet-}$. The partial reoptimization carried out for all three models resulted in moderate to appreciable reduction of the out-of-plane angles for the $Q_A^{\bullet-}$ and $Q_B^{\bullet-}$ models but in a slight increase for the $A_1^{\bullet-}$ model. Additionally, a contraction of the hydrogen bonds was observed. (cf. Table S3 in the Supporting Information).

***g*-Tensors.** Table 2 compares computed *g*-shift tensors for various models with experimental data in a variety of environments, including data[16] for the QOX Q_H site. Notably, the Δg_x value for the Q_H site is lower than data for the Q_A and Q_B sites in bacterial photosynthetic reaction centers or even for isotropic 2-propanol solution. As these reference systems feature extensive (double-sided) hydrogen bonding and a low Δg_x is representative of strong hydrogen bonding, we must conclude that the low Δg_x can only be explained by strong hydrogen bonding.

The computed Δg_x values for the models are significantly too large, and they remain too large even after scaling by 0.88 to account for systematic deficiencies of the DFT method used (cf. Computational Details). Most notably, the values remain much closer to the large gas-phase value in all models that exhibit single-sided hydrogen bonding to only one carbonyl oxygen atom. This is due to a polarization of the spin density toward the "noncoordinated" oxygen atom. Spin−orbit (SO) contributions from this oxygen atom will partly compensate for the loss of $\Delta g^{SO/OZ}$ contributions to the g_x component caused by hydrogen bonding on the other side.[30] Once we add a hydrogen bond to the second carbonyl oxygen atom, we observe immediately an appreciable lowering of Δg_x (cf. ref 30), as now the SO contributions from both oxygen atoms decrease. However, even with the most promising (asymmetric) double-sided 2/1 hydrogen-bond models (e.g., 1HO-1HN-4HO, Figure 2b), the scaled Δg_x is still about 500 ppm too large. This may be attributed to further factors, e.g., a change of the conformation of the methoxy substituents. It is known that conformational changes of the two methoxy groups may alter Δg_x by up to 600 ppm.[30] Indeed, Table 2 shows that going from the optimized structure parameters of the 1HO-1HN-4HO model (with $\theta_1 = 132°$, $\theta_2 = -57°$) to those of a fully optimized gas-phase model (with $\theta_1 = 61°$, $\theta_2 = -57°$) reduces Δg_x by about 600 ppm for the free radical (first two rows in Table 2, scaled values in parentheses). The overall effect in the presence of hydrogen bonding is probably somewhat smaller, due to the general reduction of Δg_x.[30]

Placing a +2 point charge at one of the presumed positions of the iron atom of *heme a*[20] changes the Δg_x component at

Table 2. *g*-Shift Tensors (ppm) for Ubisemiquinone Radical Anion Models

model[a]	Δg_x[b]	Δg_y	Δg_z
0/0 optimized	5466 (4810)	3282	−46
0/0 //2/1 1HO-1HN-4HO	6194 (5451)	3389	−33
0/1 4HO	5481 (4823)	3256	−56
0/1 4HN	5433 (4781)	3193	−50
1/0 1HN	5276 (4642)	3233	−44
1/0 1HO	5254 (4623)	3193	−70
2/0 1HO-1HN	4989 (4390)	3174	−59
3/0 1HO-1HO-1HN	5083 (4473)	3223	−68
1/1 1HN-4HN	4966 (4370)	3090	−71
3/1-a 1HO-1HO-1HN-4HO	4825 (4246)	3203	−121
3/1-b 1HO-1HO-1HN-4HO	4710 (4145)	3124	−36
2/2-a 1HO-1HO-4HO-4HO	4642 (4084)	2961	−129
2/2-b 1HO-1HO-4HO-4HO	4695 (4132)	3001	−88
2/1-a 1HO-1HN-4HO	4660 (4101)	3031	−105
2/1-b 1HO-1HN-4HO	4766 (4194)	3019	−92
2/1-c 1HO-1HN-4HO	4804 (4228)	3018	−84
2/1-d 1HO-1HN-4HO	4786 (4212)	3020	−58
2/1 1HN-1HN-4HN	4691 (4128)	3008	−85
1/2 1HO-4HO-4HN	4672 (4111)	3013	−81
3/2 1HO-1HO-1HN-4HO-4HN	4464 (3928)	3073	−53
2/2 1HO-1HN-4HO-4HN	4444 (3911)	3007	−80
2/3 1HO-1HN-4HO-4HO-4HN	4345 (3824)	3111	−105
Models from ref 32			
$Q_A^{\bullet-}$ (UQ-EM$^{\bullet-}$-nmf-imd-ind)[c]	5095 (4484)	3052	11
$Q_A^{\bullet-}$ (UQ-EM$^{\bullet-}$-nmf-imd)[c]	5004 (4404)	3003	26
$Q_A^{\bullet-}$ (UQ-EM$^{\bullet-}$-nmf-imd),reopt1[c]	4569 (4021)	3052	−44
$Q_A^{\bullet-}$ (UQ-EM$^{\bullet-}$-nmf-imd), reopt2[c]	4693 (4130)	3037	−50
$Q_B^{\bullet-}$ (UQ-EM$^{\bullet-}$-ind-SIG)[c]	4563 (4015)	2890	48
$Q_B^{\bullet-}$ (UQ-EM$^{\bullet-}$-ind-SIG), reopt1[c]	4352 (3830)	2941	−82
UQ-EM$^{\bullet-}$(^{i}PrOH)$_6$[c]	4602 (4050)	2927	85
$A_1^{\bullet-}$ (EMNQ$^{\bullet-}$-nmf-ind)[c]	4428 (3897)	2675	1
$A_1^{\bullet-}$ (EMNQ$^{\bullet-}$-nmf-ind), reopt3[c]	4366 (3842)	2630	23
exptl $Q_H^{\bullet-}$ in bo_3-QOX[d]	*3611*	*3111*	*−119*
exptl $Q_A^{\bullet-}$ in Zn-bRCs[e]	4300	3100	−100
exptl $Q_A^{\bullet-}$ in Zn-bRCs[f]	4170	3000	−220
exptl $Q_B^{\bullet-}$ in Zn-bRCs[f]	3940	2950	−220
exptl UQ-10$^{\bullet-}$ in *i*PrOH[g]	4140	3100	−100
exptl UQ-3$^{\bullet-}$ in *i*PrOH[h]	3900	2940	−220
exptl UQ-3$^{\bullet-}$ in DME/MTHF[h]	4680	3050	−300
exptl $A_1^{\bullet-}$ in PS−I[i]	3900	2750	−140
exptl $A_1^{\bullet-}$ in PS−I[j]	3930	2710	−49

[a] Cf. Figure 2. [b] Values scaled by 0.88 in parentheses. [c] Supermolecular model structures adopted from ref 32: UQ-EM$^{\bullet-}$ = 5-ethyl-2,3-dimethoxy-6-methyl-1,4-benzosemiquinone; EMNQ$^{\bullet-}$ = 2-ethyl-3-methyl-1,4-naphthosemiquinone; nmf = *N*-methylformamide; imd = imidazole; ind = indole; reopt1: structure was reoptimized with the positions of all heavier atoms of H-bond donors frozen; reopt2: the same as reopt1 but with dihedral angles of methoxy groups also kept frozen; reopt3: the position of nmf was reoptimized with coordinates of all other atoms fixed; small differences of g-tensors with values of ref 32 are due to a slightly different computational level of the g-tensor calculations. [d] W-band EPR in bo_3-QOX.[16] [e] W-band EPR for zinc-substituted bRC.[26] [f] Q-band EPR in zinc substituted bRC of *Rb. shaeroides* R-26, with fully deuterated UQ-10$^{\bullet-}$.[28] [g] W-band EPR in frozen 2-propanol.[26,28] [h] Q-band EPR in 2-propanol-d_8 or DME/MTHF mixtures, respectively.[29] [i] Transient spin-polarized W-band EPR on $P_{700}^{\bullet+}A_1^{\bullet-}$ in a PS-I single crystal.[12] [j] Photoaccumulated $A_1^{\bullet-}$ at 283 GHz.[10]

(50) Asher, J. R.; Kaupp, M.; Doltsinis, N. L. Unpublished results.
(51) Hellwig, P.; Mogi, T.; Tomson, F. L.; Gennis, R. B.; Iwata, J.; Miyoshi, H.; Maentele, W. *Biochemistry* **1999**, *38*, 14683−14689.

most by 50 ppm and the Δg_y component by less than 10 ppm. This suggests that electrostatic contributions from this site should not affect our conclusions. The calculations confirm clearly that the very low Δg_x observed for the Q_H site is incompatible with single-sided hydrogen bonding. What would happen, if the hydrogen bond on the O_4 site is present but very weak? Figure S1 in the Supporting Information shows that an increase of the O···H distance increases Δg_x essentially linearly but only moderately. In going from optimized 1.80 Å to about 2.20 Å, Δg_x (scaled) for the 2/1 model changes from ca. 4100 ppm to ca. 4250 ppm and thus remains appreciably below the 4514 ppm computed for the single-sided case (cf. Table 2), with the hydrogen bond to O_4 removed completely.

Systems with even more hydrogen bonding would allow a further reduction of Δg_x by about 200 ppm. Of these models, the 3/2 model 1HO-1HO-1HN-4HO-4HN (Table 2) is still expected to provide significant asymmetry in the ^{13}C hyperfine couplings (see below). An artificial shortening of some or all hydrogen bonds to 1.60 Å in the 2/1a 1HO-1HN-4HO model reduces Δg_x maximally by 300 ppm (Table S2 in the Supporting Information), when all hydrogen bonds are short. However, this is already a very unlikely bonding situation.

Previous *g*-tensor calculations on more specific supermolecular model complexes for the $Q_A^{\bullet-}$, $Q_B^{\bullet-}$, and $A_1^{\bullet-}$ sites,[32] and for ubisemiquinone in frozen 2-propanol,[30,32] provided excellent agreement with experiment after appropriate scaling of the Δg_x component to account for systematic errors of the DFT approach used. This is confirmed by the corresponding values in Table 2 (which differ slightly from those in ref 32). Structural reoptimization provided somewhat stronger intermolecular interactions compared to the initial structures (cf. Table S3 in the Supporting Information). Consequently, the g_x components are also lowered slightly more. This is most pronounced for the $Q_A^{\bullet-}$ model (Table 2): The scaled Δg_x component for the "reopt1" structure is now somewhat below experiment. It is possible that this model overestimates the strength of the hydrogen bonds now compared to the situation in the protein. The effect is smaller for the $Q_B^{\bullet-}$ model. While the *g*-tensor for this model agrees excellently with experiment, the hyperfine tensors do not (see discussion below). The *g*-tensor of the $A_1^{\bullet-}$ model is affected only slightly by the reoptimization of the single hydrogen bond (which shortens by 10 pm).

^{13}C-Carbonyl Hyperfine Tensors. It was the strongly different A_z components of the carbonyl ^{13}C hyperfine tensors for the C_1 and C_4 positions, and in particular the very low value for the C_4 position, that led one of us[16] to favor a single-sided hydrogen bonding model. In view of the above results for the *g*-tensors, it is thus of great interest to evaluate the compatibility of the hyperfine tensors for different models with this experimental observation. Computed ^{13}C hyperfine tensors are shown in Table 3, in comparison with experimental data for a variety of environments.

As A_x and A_y are determined less accurately by the measurements,[16] we concentrate in particular on the better defined A_z values. Comparison of the data for the Q_H site with frozen protic solution demonstrates the pronounced asymmetry for the two carbonyl sites. The A_z value at C_4 is indeed comparable to measurements in aprotic solvent mixtures (DME/mTHF; Table 3), where hydrogen bonding must be presumed absent.

However, our computations show that single-sided hydrogen bonding would cause an even much larger asymmetry than observed for the Q_H site, and in particular an even much lower A_z for the C_4 position. This may be understood from the strongly asymmetric and alternating spin density distribution in the single-sided case, which places relatively large positive spin density on O_4 but very low spin density on C_4. In contrast, unsymmetrical double-sided models provide much better agreement with the measured data for the Q_H site. This holds in particular for the 2/1 models 1HO-1HN-4HO or 1HN-1HN-4HN, which agree rather well with experimental data for the Q_H site. 3/1 models appear to provide too asymmetrical hyperfine couplings. Thus, not only do the computations provide better agreement with experimental *g*-tensors of Q_H when allowing double-sided yet asymmetrical hydrogen bonding, but also the characteristic carbonyl ^{13}C hyperfine tensors are reproduced more faithfully by 2/1 models. Notably, the 3/2 model does provide somewhat too large A_z components but also a reasonable asymmetry between C_1 and C_4.

Turning to the A_x and A_y components in the Q_H site, we note that, due to inherent inaccuracies in their experimental determination, the observed differences between A_x and A_y indeed may not be reliable, and even the absolute values may vary somewhat upon varying the simulation parameters (without affecting the overall quality of the spectral simulation).[16] Based on knowledge from other semiquinone spectra and computations, one would expect more negative A_x and A_y components for that *ipso*-carbon atom with the lower spin density (that is, the one bonded to the oxygen atom that experiences less hydrogen bonding). This is due to accumulation of spin density on the neighboring oxygen and *ortho*-carbon atoms (as demonstrated by spin density distributions for various model complexes provided in Figure S3 in the Supporting Information). A lower A_z component should thus be accompanied by more negative A_x and A_y components. This can be observed, e.g., in the experimental data for the Q_A and Q_B sites (Table 3). It is thus conceivable that the A_x and A_y components in the Q_H site should be significantly more negative at C_4 than at C_1. Notably, calculations for single-sided models provide not only unrealistically small A_z values but also unrealistically large absolute A_x and A_y values at the position of low spin density. Indeed, this effect becomes more pronounced when going from, e.g., the 1/0 to 2/0 and 3/0 models (Table 3). The 2/1 or 3/2 models perform better also in this respect.

We have again evaluated the effect of a successive lengthening of the hydrogen bond to O_4 in the double-sided 2/1 model 1HO-1HN-4HO (Figure S2 in the Supporting Information). Going from a hydrogen bond distance of 1.80 Å to 2.20 Å, A_z in the C_1 position increases slightly toward the experimental value 30.8 MHz, but in the C_4 position it decreases below the observed 20.2 MHz. These calculations provide thus no indications for or against a somewhat weakened hydrogen bond on the O_4 side.

We have also performed calculations for the 2/1 model 1HO-1HN-4HO with a +2 point charge at the *heme-a* iron position. Depending on the orientation of the semiquinone in the putative binding site, slightly different relative arrangements of the point charges and the semiquinone arise (see Table S1 in the Supporting Information for coordinates). For different orientations chosen, the A_z values of C_1 vary between 27.74 and 29.74

Table 3. ^{13}C Hyperfine Coupling Tensors (in MHz) for the C1 and C4 Carbonyl Positions in Ubisemiquinone Radical Anion Models

	^{13}C-HFC at C_1			^{13}C-HFC at C_4		
model[a]	A_x	A_y	A_z	A_x	A_y	A_z
0/0 optimized	−12.8	−16.3	14.0	−12.9	−16.4	14.1
0/0 //2/1 1HO-1HN-4HO	−15.0	−18.8	6.4	−11.3	−14.6	16.8
0/1 4HO	−16.4	−20.5	1.5	−8.5	−11.2	31.0
0/1 4HN	−16.8	−20.9	0.9	−8.3	−10.9	32.3
1/0 1HN	−11.4	−14.4	24.3	−13.7	−17.4	10.1
1/0 1HO	−10.5	−13.4	25.6	−14.4	−18.1	9.4
2/0 1HO-1HN	−9.0	−11.4	37.0	−14.9	−18.6	6.6
3/0 1HO-1HO-1HN	−7.3	−9.5	41.5	−15.9	−19.9	3.5
1/1 1HN-4HN	−14.0	−17.3	15.8	−10.5	−13.3	25.9
3/1-a 1HO-1HO-1HN-4HO	−9.4	−11.7	37.0	−13.7	−17.0	12.9
3/1-b 1HO-1HO-1HN-4HO	−9.0	−11.3	38.6	−13.6	−16.9	15.2
2/2-a 1HO-1HO-4HO-4HO	−11.7	−14.6	24.7	−11.8	−14.7	24.6
2/2-b 1HO-1HO-4HO-4HO	−12.6	−15.5	20.8	−11.6	−14.4	26.5
2/1-a 1HO-1HN-4HO	−11.2	−14.0	27.9	−12.0	−15.0	20.8
2/1-b 1HO-1HN-4HO	−11.1	−13.9	26.1	−12.6	−15.7	20.8
2/1-c 1HO-1HN-4HO	−11.0	−13.8	26.7	−13.1	−16.4	18.5
2/1-d 1HO-1HN-4HO	−10.8	−13.4	27.9	−13.5	−16.7	18.5
2/1 1HN-1HN-4HN	−11.6	−14.4	27.9	−12.0	−15.0	20.8
1/2 1HO-4HO-4HN	−13.4	−16.7	18.2	−10.0	−12.6	30.3
3/2 1HO-1HO-1HN-4HO-4HN	−11.3	−13.8	33.6	−11.3	−14.0	25.3
2/2 1HO-1HN-4HO-4HN	−13.6	−16.5	23.1	−10.3	−12.8	29.7
2/3 1HO-1HN-4HO-4HO-4HN	−14.6	−17.7	19.4	−7.6	−9.6	40.1
			Models from ref 32			
$Q_A^{\bullet-}$ (UQ-EM$^{\bullet-}$-nmf-imd-ind)[b]	−13.7	−17.1	16.3	−10.7	−13.7	23.0
$Q_A^{\bullet-}$ (UQ-EM$^{\bullet-}$-nmf-imd)[b]	−13.6	−17.1	16.6	−11.1	−14.1	22.6
$Q_A^{\bullet-}$ (UQ-EM$^{\bullet-}$-nmf-imd), reopt1[b]	−14.5	−17.9	16.0	−10.0	−12.6	28.0
$Q_A^{\bullet-}$ (UQ-EM$^{\bullet-}$-nmf-imd), reopt2[b]	−13.6	−17.0	15.5	−10.2	−13.1	26.4
$Q_B^{\bullet-}$ (UQ-EM$^{\bullet-}$-ind-SIG)[b]	−11.0	−13.9	26.5	−13.4	−16.7	18.8
$Q_B^{\bullet-}$ (UQ-EM$^{\bullet-}$-ind-SIG), reopt1[b]	−11.4	−14.2	28.6	−12.1	−15.1	21.6
UQ-EM$^{\bullet-}$(^{i}PrOH)$_6$[b]	−11.7	−14.4	26.9	−12.1	−14.9	26.4
$A_1^{\bullet-}$ (EMNQ$^{\bullet-}$-nmf-ind)[b]	−11.3	−14.3	21.3	−13.0	−16.4	11.0
$A_1^{\bullet-}$ (EMNQ$^{\bullet-}$-nmf-ind), reopt3[b]	−10.5	−13.3	26.0	−13.4	−16.8	9.9
exptl $Q_H^{\bullet-}$ in bo_3-QOX[c]	*−4.2 (14)*	*−12.6 (14)*	*30.8 (8)*	*−7.0 (14)*	*−10.4 (14)*	*20.2 (8)*
exptl $Q_A^{\bullet-}$ in Zn-bRCs[d]	−12.6(17)	−14.6(17)	22.7 (6)	−9.2 (17)	−9.8 (17)	35.0 (6)
exptl $Q_A^{\bullet-}$ in Zn-bRCs[e]	15.4 (14)	18.2 (14)	22.4 (8)	<7.0 (14)	<7.0 (14)	35.6 (8)
exptl $Q_B^{\bullet-}$ in Zn-bRCs[d]	−10.9 (17)	−13.2 (17)	27.7 (6)	−10.1 (17)	−10.4 (17)	32.2 (6)
exptl UQ-3$^{\bullet-}$ in *i*PrOH[d]	−12.1 (17)	−10.4 (17)	30.6 (6)	−11.2 (17)	−9.8 (17)	32.2 (6)
exptl UQ-10$^{\bullet-}$ in *i*PrOH[e]	n.d.	n.d.	31.7 (8)	n.d.	n.d.	30.8 (8)
exptl UQ-3$^{\bullet-}$ in DME/MTHF[f]	−12.1 (22)	−15.1 (22)	20.5 (6)	−13.2 (22)	−15.4 (22)	20.5 (6)
exptl 2-methyl-NQ in PS-I[g]	−10.5 (15)	−10.5 (15)	44.0 (20)	n.d.	n.d.	n.d.
calcd $VK_1^{\bullet-}$[h]	−12.2	−15.1	22.2	−16.6	−20.4	1.5

[a] Cf. Figure 2. Atom labels for A_1 converted in analogy to the numbering used for ubisemiquinone models. [b] Structures adapted from ref 32; see footnote c of Table 2. [c] Native UQ-8 substituted with ^{13}C selectively labeled UQ-2.[16] [d] Native UQ-10 substituted with selectively ^{13}C labeled UQ-3 (cf. ref 52). [e] With selectively ^{13}C-labeled UQ-10.[53] [f] Reference 29. [g] From simulations of Q- and X-band transient radical pair spectra for 2-methyl-naphthoquinone in the A_1 binding site.[54] [h] B3LYP/EPR-II calculations on an A_1 model made from vitamin K_1 and a methyl-imidazole molecule H-bonded to O_4.[55]

MHz, and those for C_4, between 17.70 and 18.00 MHz. There is thus an electrostatic influence on these carbonyl ^{13}C couplings. However, it is not large enough to favor any of the other models for the hydrogen-bonding environment. Models with artificially *shortened* hydrogen bonds provide generally too high values for A_z of C_1 and too low ones for C_4 (Table S2 in the Supporting Information). An exception is due to the model where only one O_1···OH bond is shortened. This model provides good agreement with the experimental values.

We may also compare our computed hyperfine values to experimental values from other, structurally better characterized protein sites (Table 3). In comparison with the bacterial Q_A site, a 1/1 model provides overall too low A_z values but gives the right type of asymmetry. A 2/3 model exhibits a somewhat larger asymmetry in A_z than measured, as well as rather reasonable A_x and A_y components. While the 2/3 complex is far from the experimentally observed structure,[3,8] it does thus seem to model the spin-density distribution in the Q_A site well. In fact, it appears to be generally accepted that, of the two hydrogen bonds to O_1 and O_4, the O_4···histidine one is stronger.[4,56] The $Q_A^{\bullet-}$ model from ref 32, with or without π-stacked indole (to model a tryptophan residue), gives a lower asymmetry. The asymmetry is better reproduced after reoptimization of the structure (cf. entries reopt 1 and reopt 2 in Table 3), but both A_z components remain too low (absolute A_x and A_y values tend in turn to be overestimated, in agreement with the discussion above).

Experimental data for the Q_B site are also best reproduced by the 2/3 model. The supermolecular model for $Q_B^{\bullet-}$ model from ref 32 was based on an X-ray structure for the charge-separated $P^+Q_B^{\bullet-}$ state at 2.6 Å resolution.[3] It reproduces well

(52) Isaacson, R. A.; Abresch, E. C.; Lendzian, F.; Boullais, C.; Paddock, M. L.; Mioskowski, C.; Lubitz, W.; Feher, G. In *The reaction center of photosynthetic bacteria, structure and dynamics*; Michael-Beyerle, M.-E., Eds.; Springer-Verlag: Berlin, Germany, 1996; pp 353−367.
(53) van den Brink, J. S.; Spoyalov, A. P.; Gast, P.; van Liemt, W. B. S.; Raap, J.; Lugtenburg, J.; Hoff, A. J. *FEBS Lett.* **1994**, *353*, 273−276.
(54) Pushkar, Y. N.; Golbeck, J. H.; Stehlik, D.; Zimmermann, H. *J. Phys. Chem. B* **2004**, *108*, 9439−9448.
(55) O'Malley, P. J. *Biochim. Biophys. Acta* **1999**, *1411*, 101−113.
(56) Pushkar, Y. N.; Ayzatulin, O.; Stehlik, D. *Appl. Magn. Reson.* **2005**, *28*, 195−211.

the *g*-tensor (see above). However, the asymmetry in the carbonyl ^{13}C A_z components has the wrong sign (albeit reasonable magnitude, cf. Table 3). Reoptimization of the structure increases both A_z components slightly but does not reverse the asymmetry. We suspect that the very hydrophilic environment within the Q_B site provides a highly dynamical hydrogen-bonding situation that is not adequately described by the static model from ref 32.

The phyllosemiquinone A_1 site in PS-I has only been studied so far using 2-methyl-naphthoquinone ^{13}C-labeled at the C_1 position (Table 3). The authors state that this molecule is bound with the same orientation as the native phylloquinone and thus can be used as a model system. Spectral simulation of the transient radical pair spectra at two microwave frequencies are used to determine the observed HFCs. While it is clear that the magnitude of A_z is about 40 MHz (see Table 3), the other two components of the hyperfine tensor are quite difficult to determine with much degree of accuracy from such spectra. Moreover, it is unclear to what extent the missing extended side chain might affect the hydrogen-bonding framework and thus the spin-density distribution. The results obtained with the $A_1^{\bullet-}$ model from ref 32 provide an appreciable asymmetry but a significantly too low A_z value for C_1. Other supermolecular model DFT calculations by O'Malley[55] on a complex between vitamin K_1 (i.e., the phytyl side chain of phylloquinone was replaced by a propene moiety) H-bonded at O_1 (when using analogous atom labeling as shown for ubisemiquinone in Figure 2) to a methylimidazole molecule (Table 3) provide a similar A_z for C_1 but a still lower A_z at C_4 (and a more negative A_{iso} at that position). While no structural data were provided in ref 55, the otherwise almost identical computational level makes us suspect that a very short hydrogen bond had been chosen to provide such a large asymmetry (see discussion below for ^1H and ^{17}O HFCs).

In comparison with isotropic protic solution results, computed data for symmetrical 2/2 models depend also sensitively on the particular minimum structure used (cf. entries 2/2-a and 2/2-b in Table 3). They may provide symmetrical HFCs or unsymmetrical ones, in the latter case with $A_z(C_4) > A_z(C_1)$. The UQ-EM$^{\bullet-}$(^{i}PrOH)$_6$ model from ref 32 provides symmetrical HFCs, somewhat below the experimental values. It is clear that the identical values observed for the two positions in frozen solution reflect dynamical or statistical averaging. Another interesting result is the almost vanishing A_z at C_1 for 0/1 models. A general conclusion is that one may not use measurements in a completely symmetrical situation (e.g., in protic or aprotic solvents) to estimate the carbonyl HFCs in unsymmetrical situations. The asymmetric spin density distribution in the latter case may lead to very different hyperfine data.

^{1}H(CH$_3$) Hyperfine Tensors. Table 4 shows the ^1H HFC tensors of the methyl group in the C_5-position, averaged over all three hydrogen atoms.[57] As expected and found experimentally,[4,58] the largest component, A_y, is oriented roughly along the C_5-C(methyl) bond, and the tensor is almost but not quite axial, consistent with the structure of the radical (cf. Figure 1). These ^1H HFC tensors are the only quantity that appears to be slightly better described by a single-sided 2/0 model than by double-sided 2/1 models (Table 4). In the latter case, all three components (and thus the isotropic value) are about 2−3 MHz too low relative to the observed value, whereas the 2/0 model is slightly closer to experiment. A 3/1 model (Table 4) also provides somewhat larger values. Interestingly, also the 3/2 model provides slightly better agreement with experiment than the 2/1 models. Lengthening of the hydrogen bond to O_4 to about 2.20 Å in the 2/1-a 1HO-1HN-4HO model increases the three values by only about 0.3 MHz. Introduction of the +2 point charge at the suspected position of the *heme-a* iron atom changes the tensor components by at most 0.5 MHz and thus cannot account for the discrepancies between the 2/1 models and experiment. Shortening of the hydrogen bonds to 1.60 Å

Table 4. 5-Methyl ^1H Hyperfine Coupling Tensors HFC (in MHz)[a]

	^{1}H-HFC		
model[b]	A_x	A_y	A_z
0/0 opt	4.9	8.3	3.9
0/0 from best model	4.7	8.1	3.8
0/1 4HO	2.8	5.9	1.8
0/1 4HN	2.6	5.8	1.7
1/0 1HN	6.4	10.2	5.5
1/0 1HO	6.2	9.9	5.3
2/0 1HO-1HN	7.8	11.5	6.8
3/0 1HO-1HO-1HN	8.0	11.9	7.1
1/1 1HN-4HN	4.3	7.7	3.5
3/1-a 1HO-1HO-1HN-4HO	7.1	10.8	6.2
3/1-b 1HO-1HO-1HN-4HO	7.7	11.5	6.8
2/2-a 1HO-1HO-4HO-4HO	5.0	8.5	4.2
2/2-b 1HO-1HO-4HO-4HO	3.7	7.1	2.9
2/1-a 1HO-1HN-4HO	5.9	9.5	5.1
2/1-b 1HO-1HN-4HO	5.1	8.6	4.2
2/1-c 1HO-1HN-4HO	5.2	8.8	4.3
2/1-d 1HO-1HN-4HO	5.3	8.8	4.4
2/1 1HN-1HN-4HN	6.0	9.7	5.2
1/2 1HO-4HO-4HN	3.9	7.2	3.0
3/2 1HO-1HO-1HN-4HO-4HN	6.4	10.0	5.6
2/2 1HO-1HN-4HO-4HN	4.8	8.2	4.0
2/3 1HO-1HN-4HO-4HO-4HN	4.0	7.3	3.2
Models from ref 32			
$Q_A^{\bullet-}$ (UQ-EM$^{\bullet-}$-nmf-imd-ind)[c]	3.9	7.0	3.0
$Q_A^{\bullet-}$ (UQ-EM$^{\bullet-}$-nmf-imd)[c]	4.6	7.9	3.7
$Q_A^{\bullet-}$ (UQ-EM$^{\bullet-}$-nmf-imd), reopt1[c]	4.8	8.2	3.8
$Q_A^{\bullet-}$ (UQ-EM$^{\bullet-}$-nmf-imd), reopt2[c]	4.0	7.3	3.1
$Q_B^{\bullet-}$ (UQ-EM$^{\bullet-}$-ind-SIG)[c]	5.3	8.9	4.4
$Q_B^{\bullet-}$ (UQ-EM$^{\bullet-}$-ind-SIG), reopt1[c]	0.0	2.1	−0.4
UQ-EM$^{\bullet-}$ + (^{i}PrOH)$_6$[c]	4.0	7.3	3.2
$A_1^{\bullet-}$ (EMNQ$^{\bullet-}$-nmf-ind)[c]	6.9	10.5	6.0
$A_1^{\bullet-}$ (EMNQ$^{\bullet-}$-nmf-ind), reopt3[c]	7.6	11.3	6.7
exptl $Q_H^{\bullet-}$ in bo_3-QOX[d]	*8.40*	*12.78*	*7.85*
exptl $Q_A^{\bullet-}$ in Zn-bRCs[e]	3.8 (1)	6.9 (1)	3.2 (1)
exptl $Q_B^{\bullet-}$ in Zn-bRCs[e]	4.4 (1)	7.8 (1)	3.9 (1)
exptl UQ-0$^{\bullet-}$ in *i*PrOH[f]	4.8 (3)	9.0 (3)	4.8 (3)
exptl UQ-3$^{\bullet-}$ in *i*PrOH[f]	5.3 (3)	8.4 (3)	5.0 (3)
exptl UQ-10$^{\bullet-}$ in *i*PrOH[g]	4.8	8.5	4.8
exptl UQ-0$^{\bullet-}$ in DME/mTHF[f]	5.0 (3)	8.4 (3)	5.0 (3)
exptl UQ-3$^{\bullet-}$ in DME/mTHF[f]	5.0 (3)	8.1 (3)	5.0 (3)
exptl UQ-10$^{\bullet-}$ in DME/mTHF[h]	5.2 (3)	8.4 (3)	5.2 (3)
exptl A$^{\bullet-}$ in PS-I[i]	9.0	12.6	9.0
exptl $A_1^{\bullet-}$ in PS I[j]	8.9 (1)	12.5 (1)	8.9 (1)
calcd $VK_1^{\bullet-}$[k]	9.2	12.6	8.2

[a] Cf. Figure 1 for atom labels. Atom labels for A_1 converted in analogy to the numbering used for ubisemiquinone models. Average HFCs for the three hydrogen atoms. [b] Cf. Figure 2. [c] Structures adapted from ref 32; see footnote c of Table 2. [d] Reference 24. [e] Reference 4. [f] X-band ENDOR and X- and Q-band EPR simulations.[29] [g] Reference 37. [h] Reference 59. [i] Reference 60. [j] Transient spin-polarized ENDOR.[61] [k] B3LYP/EPR-II calculations on an A_1 model made from vitamin K_1 and a methyl-imidazole molecule H-bonded to O_4.[55]

(57) Mattar, S. M. *J. Phys. Chem. B* **2004**, *108*, 9449−9455.
(58) Rohrer, M.; MacMillan, F.; Prisner, T. F.; Gardiner, A. T.; Möbius, K.; Lubitz, W. *J. Phys. Chem. B* **1998**, *102*, 4648−4657.

increases the HFC tensor components by up to 1 MHz (Table S2 in the Supporting Information).

We may again also compare results from the more sophisticated X-ray structure-based models from ref 32 with the corresponding experimental HFC tensors (Table 4). The $Q_A^{\bullet-}$ model without reoptimization provides excellent agreement with experiment. Removal of the indole residue increases all components by about 0.8 MHz. Full reoptimization of this reduced model ("reopt1") has little effect, whereas reoptimization under freezing of the methoxy conformation ("reopt2") decreases the results somewhat. The $Q_B^{\bullet-}$ binding site model from ref 32 provides results slightly above experiment, whereas structure reoptimization leads to unrealistically low values (this confirms our above conclusion that the X-ray structure for the charge-separated $P^+Q_B^{\bullet-}$ state[3] may not reflect well the dynamical hydrogen-bonding situation in this hydrophilic site; see discussion above). An underestimate by ca. 2 MHz for all three components is found for the $A_1^{\bullet-}$ model, but reoptimization increases the HFCs slightly toward experiment. Here the vitamin K_1/methyl-imidazole model of O'Malley[55] provides larger values (at the same computational level). As discussed above for the ^{13}C HFCs, this may reflect a choice of a very short hydrogen bond length and thus a more asymmetric spin-density distribution than our best optimized models provide. The UQ-$EM^{\bullet-}$(^{i}-PrOH)$_6$ model underestimates experimental values for ubisemiquinone in frozen 2-propanol also by about 1−2 MHz.

It seems easy to be off by a few MHz in either direction for these ^1H HFCs, even with relatively realistic models. It appears that these $^1H(CH_3)$ couplings are generally more sensitive to small (unsymmetrical) changes in the wider environment of the semiquinone than, e.g., ^{13}C HFCs or *g*-tensors. For example, the experimental $^1H(CH_3)$ HFCs for the Q_H site in Table 4 are for a pH of 6 but increase by about 2 MHz upon going to pH 8 (for all components).[59] In view of the results for other binding sites and other model complexes, and based on the relatively modest differences between models, we do not think that the $^1H(CH_3)$ HFCs provide strong evidence for a single-sided model either.

^{1}H Hyperfine Tensors for Hydrogen-Bonded Protons. Table 5 provides ^1H HFCs for the hydrogen-bonded protons, together with some experimental values for semiquinones in different environments. A few general trends related to the structures in Table 1 may be noted from the computed values. (a) Larger A_{33} values (> 6 MHz) are associated with short hydrogen bonds, whereas the hydrogen bonds above 2 Å tend to exhibit values around 4−5 MHz. The particularly large A_{33} values in some of the quoted experimental cases (in particular $Q_A^{\bullet-}$ in bacterial reaction centers, but also the $A_1^{\bullet-}$ site in photosystem I) suggest thus a rather short and strong hydrogen bond, in agreement with observation. (b) As one might expect, essentially dipolar tensors (with A_{iso} < 1 MHz) are found in particular for hydrogen bonds close to the ring plane (or in one case for an extremely out-of-plane hydrogen bond, cf. 3/1-b model), whereas the hydrogen bonds with γ values between ca. 20°−60° tend to exhibit larger isotropic contributions. This is well-known from ENDOR measurements.[4,37,58,62] Among the experimental examples included, isotropic contributions are particularly notable for UQ-$10^{\bullet-}$ in 2-propanol, where they suggest a substantial out-of-plane orientation of the measured proton.

In the context of the Q_H site, it is notable that the 3/2 model exhibits one distinctly larger hyperfine anisotropy (1OH position) than any of the 2/1 models, combined with an appreciably negative isotropic value. From H_2O/D_2O exchange ENDOR experiments, Hasting et al.[23] indicated exchangeable proton hyperfine features of $A_\perp = -5.1$ MHz and $A_\parallel = 11.7$ MHz and suggested strong out-of-plane hydrogen bonding. This would be consistent with three hydrogen bonds to O_1. An improved identification of the hydrogen-bonding environment might be obtained from orientation-selective ENDOR, possibly at higher frequencies or using two-dimensional pulsed EPR (HYSCORE).

^{17}O-Hyperfine Tensors. No ^{17}O carbonyl hyperfine couplings have as yet been measured for semiquinones in QOX. Table 6 provides predicted values for the different supermolecular model complexes. Assuming a 2/1 double-sided model, the difference between the O_1- and O_4-position is only about 1.5−2.0 MHz for all three components, with the value for O_1 being lower. That is, mainly the isotropic HFC differs between the two oxygen centers. The single-sided 2/0 model provides a much larger difference of about 20 MHz for A_z, whereas the A_x and A_y components are about 6 MHz more negative on O_4 than on O_1 (Table 6). 3/1 models give about 15 MHz more negative A_z and about 4 MHz more negative A_x and A_y values on O_4. The addition of a double point charge at the presumed *heme-a* iron position in the 2/1 1HO-1HN-4HO model reduces $A_z(O_1)$ by about 2 MHz and increases $A_z(O_4)$ by about the same amount. The asymmetry is thus potentially increased by the electrostatic effect of the *heme-a* group maximally from about 2 MHz to about 6 MHz. It seems that the ^{17}O HFCs (of suitably labeled samples) reflect the hydrogen-bonding situation less than the corresponding ^{13}C HFCs (see above and ref 56). Whether they may be of diagnostic value will depend on the experimental resolution available (see below).

When turning to ubisemiquinone sites with experimentally known ^{17}O HFCs (Table 6), we note that the ca. 18 MHz larger A_z for O_1 for $Q_A^{\bullet-}$ is somewhat underestimated (ca. 11 MHz) by a 1/1 model (which is close to the actually observed structure), as the A_z value or O_4 is too negative. The more sophisticated $Q_A^{\bullet-}$ model from ref 32 provides a similar asymmetry (12−13 MHz) but even slightly larger absolute values. Reoptimization of this model enhances the asymmetry and provides thus better agreement with experiment (with somewhat too large absolute values, cf. entry "reopt1"). On the other hand, the resolution of the experimental asymmetry is somewhat uncertain anyway (and the assignment to the two positions was based on the related ^{13}C data).[4]

Experimental uncertainties are even more pronounced for the Q_B site, where the asymmetry has been obtained from the simulation of a single peak that was about 30% broader than that for Q_A at the same experimental conditions. None of the

(59) MacMillan, F.; Teutloff, C.; Boullais, C. Unpublished results.

(60) Rigby, S. E.; Evans, M. C.; Heathcote, P. *Biochemistry* **1996**, *35*, 6651−6656.
(61) Teutloff, C.; Bittl, R.; Lubitz, W. *Appl. Magn. Reson.* **2004**, *26*, 5−21.
(62) Pushkar, Y. N.; Stehlik, D.; van Gastel, M.; Lubitz, W. *J. Mol. Struct.* **2004**, *700*, 233−241.
(63) O'Malley, P. J.; Babcock, G. T. *J. Am. Chem. Soc.* **1986**, *108*, 3995−4001.
(64) Flores, M.; Isaacson, R. A.; Calvo, R.; Feher, G.; Lubitz, W. *Chem. Phys.* **2003**, *294*, 401−413.

Table 5. ^{1}H Hyperfine Couplings (in MHz) for Exchangeable Hydrogens

model[a]	H-bond[a]	^{1}H-HFC (MHz) A_{11}	A_{22}	A_{33}	model[a]	H-bond[a]	^{1}H-HFC (MHz) A_{11}	A_{22}	A_{33}
0/1 4HO	4HO	−5.6	−5.3	7.2	2/1-b 1HO-1HN-4HO	1HO	−3.4	−3.1	6.3
0/1 4HN	4HN	−3.0	−2.4	6.0		1HN	−2.5	−2.4	5.2
1/0 1HN	1HN	−3.5	−3.4	6.5		4HO	−4.4	−4.2	6.9
1/0 1HO	1HO	−3.6	−3.2	6.5	2/1-c 1HO-1HN-4HO	1HO	−3.3	−2.9	6.2
2/0 1HO-1HN	1HO	−6.1	−5.7	7.2		1HN	−2.5	−2.4	5.3
	1HN	−3.2	−3.1	5.8		4HO	−4.4	−4.2	6.8
3/0 1HO-1HO-1HN	1HO	−3.6	−3.5	4.3	2/1-d 1HO-1HN-4HO	1HO	−4.1	−3.9	6.5
	1HO	−3.7	−3.3	5.7		1HN	−3.0	−2.8	5.5
	1HN	−4.9	−4.3	6.4		4HO	−5.0	−4.9	7.1
1/1 1HN-4HN	1HN	−3.0	−2.9	6.4	2/1 1HN-1HN-4HN	1HN	−2.9	−2.6	6.0
	4HN	−3.4	−3.0	6.6		1HN	−2.4	−2.2	5.2
3/1-a 1HO-1HO-1HN-4HO	1HO	−3.6	−3.5	4.4		4HN	−3.4	−3.0	6.6
	1HO	−4.1	−3.6	6.0	1/2 1HO-4HO-4HN	1HO	−2.1	−1.0	4.5
	1HN	−5.0	−4.5	6.3		4HO	−2.9	−2.6	6.0
	4HO	−4.9	−4.4	6.4		4HN	−3.6	−3.4	5.8
3/1-b 1HO-1HO-1HN-4HO	1HO	−2.1	−2.0	4.4	3/2 1HO-1HO-1HN-4HO-4HN	1HO	−6.8	−6.4	7.8
	1HO	−6.5	−6.0	7.8		1HO	−2.4	−2.3	4.6
	1HN	−2.3	−2.1	4.8		1HN	−2.4	−2.1	4.9
	4HO	−5.0	−4.8	7.0		4HO	−3.1	−2.8	6.1
2/2-a 1HO-1HO-4HO-4HO	1HO	−3.2	−3.7	6.5		4HN	−4.1	−3.8	5.9
	1HO	−2.4	−2.3	4.5	2/2 1HO-1HN-4HO-4HN	1HO	−3.3	−2.9	6.6
	4HO	−2.2	−2.2	4.5		1HN	−2.6	−2.4	5.7
	4HO	−3.8	−3.3	6.8		4HO	−3.1	−2.9	6.1
2/2-b 1HO-1HO-4HO-4HO	1HO	−3.8	−3.7	6.4		4HN	−4.1	−3.8	6.0
	1HO	−3.3	−3.2	4.6	2/3 1HO-1HN-4HO-4HO-4HN	1HO	−3.2	−2.8	6.7
	4HO	−2.3	−2.2	4.5		1HN	−2.6	−2.4	5.7
	4HO	−3.3	−2.8	6.6		4HO	−4.0	−3.7	5.2
2/1-a 1HO-1HN-4HO	1HO	−3.4	−3.1	6.3		4HO	−5.9	−4.8	6.3
	1HN	−2.5	−2.4	5.4		4HN	−3.3	−2.9	5.0
	4HO	−4.3	−4.1	6.7					
					Models from ref 32				
$Q_A^{\bullet-}$ (UQ-EM$^{\bullet-}$-nmf-imd-ind)[b]	1HN	−6.5	−6.2	8.2		1HN	−1.9	−1.3	3.3
	4HN	−5.4	−5.2	8.0		4HN	−3.4	−3.0	6.5
$Q_A^{\bullet-}$ (UQ-EM$^{\bullet-}$-nmf-imd)[b]	1HN	−6.4	−6.1	8.2	UQ-EM$^{\bullet-}$(^{i}PrOH)$_6$[b]	1HO	−5.7	−5.6	7.0
	4HN	−5.4	−5.2	8.0		1HO	−3.4	−3.1	6.5
$Q_A^{\bullet-}$ (UQ-EM$^{\bullet-}$-nmf-imd), reopt1[b]	1HN	−4.5	−4.3	6.9		4HO	−7.2	−6.8	7.1
	4HN	−4.7	−4.5	7.3		4HO	−4.0	−3.7	6.7
$Q_A^{\bullet-}$ (UQ-EM$^{\bullet-}$-nmf-imd), reopt2[b]	1HN	−4.7	−4.7	7.2	$A_1^{\bullet-}$ (EMNQ$^{\bullet-}$-nmf-ind)[b]	1HN	−2.5	−2.2	5.9
	4HN	−4.9	−4.7	7.6	$A_1^{\bullet-}$ (EMNQ$^{\bullet-}$-nmf-ind), reopt3[b]	1HN	−3.4	−2.9	6.4
$Q_B^{\bullet-}$ (UQ-EM$^{\bullet-}$-ind-SIG)[b]	1HO	−2.2	−2.1	3.8	exptl UQ-10$^{\bullet-}$ in ^{i}PrOH[c]	HO	−1.33	−1.33	6.00
	1HN	−4.2	−4.0	5.8	exptl BQ$^{\bullet-}$ in ^{i}PrOH[d]	HO	−2.8	−2.8	5.9
	1HN	−2.0	−1.4	3.3	exptl BQ$^{\bullet-}$ in H_2O[e]	HO	−2.66	−2.67	6.36
	4HN	−4.5	−4.2	7.3	exptl $Q_A^{\bullet-}$ in Zn-bRCc[f]	HN	(−)4.6	(−)4.6	8.9
$Q_B^{\bullet-}$ (UQ-EM$^{\bullet-}$-ind-SIG), reopt1[b]	1HO	−2.6	−2.2	4.8	exp. deuterated 2-methyl-NQ in PS-I[g]	HN	−4.9	−4.9	7.7
	1HN	−4.3	−4.1	5.7					

[a] Cf. Figure 2. [b] Structures adapted from ref 32; see footnote c of Table 2. [c] From ENDOR difference spectra (protonated minus deuterated 2-propanol).[37] [d] Reference 63. [e] Reference 64. [f] Reference 4. [g] Reference 62.

models studied appears to reproduce the smaller asymmetry for $Q_B^{\bullet-}$ particularly well. The $Q_B^{\bullet-}$ model from ref 32 exhibits the wrong sign of the asymmetry, and reoptimization worsens matters. Apart from the experimental uncertainties, it is also possible that the spin density distribution in the very flexible Q_B site is not well represented by the particular static model used (see discussion above).

In the case of 2-methyl-naphthosemiquinone in the A_1 site of PS-I (Table 6), the A_1 models of ref 32 give reasonable asymmetry, particularly after reoptimization ("reopt3"). The vitamin K_1/methyl-imidazole model of O'Malley[55] for $A_1^{\bullet-}$ gives a more pronounced asymmetry (larger A_z for O_4). Again (see discussion above for ^{13}C and ^{1}H HFCs) this may reflect a choice of a very short hydrogen bond length and thus a very asymmetric spin density.

A Model for Cofactor−Protein Interactions in the Q_H Binding Site. Taking all available data into account that is available from (a) crystallography,[20] (b) functional studies of site-directed mutants,[20] (c) various EPR, ENDOR, and ESEEM studies,[16,21−24] and (d) our present quantum chemical calculations, we may propose a refined model for the binding mode of the semiquinone state in the Q_H site of *bo*$_3$ QOX. Based on the model of Abramson et al. for the binding site,[20] and accepting a double-sided 2/1 hydrogen-bonding environment with the single hydrogen bond on the O_4 side, we arrive at the tentative model shown in Figure 3, in which Asp75 and Arg71 hydrogen-bond to O_1 of the semiquinone and X represents the single hydrogen bond to O_4. In this case, His98 and Gln101 would not be involved in hydrogen bonding to the semiquinone. This choice rests on the ESEEM data:[24] coupling to a single nitrogen nucleus, assigned to a backbone peptide nitrogen,[16] while no indications for a coupling to histidine have been found. The experimental data are sufficiently specific to exclude a strong interaction to histidine, whereas a backbone peptide nitrogen and an arginine nitrogen could not be distinguished so easily. Thus, the model in Figure 3 is consistent with the

Table 6. Computed ^{17}O Hyperfine Coupling Tensors HFC (in MHz) for the O_1 and O_4 Positions

model[a]	^{17}O-HFC at O_1			^{17}O-HFC at O_4		
	A_x	A_y	A_z	A_x	A_y	A_z
0/0 optimized[b]	19.3	18.6	−96.6	19.1	18.5	−96.2
0/0 from best model[c]	22.2	21.5	−107.8	18.0	17.3	−91.9
0/1 4HO	22.3	21.7	−106.9	14.9	14.2	−82.2
0/1 4HN	22.8	22.2	−108.4	14.3	13.5	−79.8
1/0 1HN	17.1	16.3	−90.0	20.0	19.3	−99.3
1/0 1HO	15.9	15.2	−87.5	20.6	19.9	−102.6
2/0 1HO-1HN	15.0	14.2	−82.7	20.5	20.0	−98.5
3/0 1HO-1HO-1HN	13.5	12.6	−74.5	22.1	21.5	−105.5
1/1 1HN-4HN	18.9	18.2	−97.6	16.0	15.3	−86.4
3/1-a 1HO-1HO-1HN-4HO	14.7	13.9	−80.8	19.4	18.9	−95.6
3/1-b 1HO-1HO-1HN-4HO	14.4	13.7	−78.3	18.6	18.0	−95.0
2/2-a 1HO-1HO-4HO-4HO	16.3	15.5	−89.4	16.4	15.6	−91.2
2/2-b 1HO-1HO-4HO-4HO	16.8	16.0	−91.1	16.4	15.6	−90.0
2/1-a 1HO-1HN-4HO	16.3	15.5	−88.2	17.8	17.1	−91.2
2/1-b 1HO-1HN-4HO	15.5	14.8	−87.4	18.3	17.6	−94.6
2/1-c 1HO-1HN-4HO	15.6	14.8	−87.6	18.4	17.7	−95.4
2/1-d 1HO-1HN-4HO	15.1	14.4	−85.5	18.5	17.9	−95.6
2/1 1HN-1HN-4HN	16.2	15.4	−89.2	17.0	16.4	−90.0
1/2 1HO-4HO-4HN	18.6	18.0	−97.9	14.7	14.0	−82.6
3/2 1HO-1HO-1HN-4HO-4HN	15.7	15.0	−84.9	15.2	14.6	−85.0
2/2 1HO-1HN-4HO-4HN	17.2	16.5	−95.8	14.3	13.7	−81.4
2/3 1HO-1HN-4HO-4HO-4HN	18.2	17.5	−98.5	12.7	12.0	−71.0
Models from ref 32						
$Q_A^{\bullet-}$ (UQ-EM$^{\bullet-}$-nmf-imd-ind)[d]	18.8	18.2	−94.8	14.7	14.1	−82.4
$Q_A^{\bullet-}$ (UQ-EM$^{\bullet-}$-nmf-imd)[d]	18.4	17.8	−95.3	14.7	14.1	−83.1
$Q_A^{\bullet-}$ (UQ-EM$^{\bullet-}$-nmf-imd), reopt1[d]	19.2	18.6	−98.0	14.6	13.9	−79.6
$Q_A^{\bullet-}$ (UQ-EM$^{\bullet-}$-nmf-imd), reopt2[d]	18.9	18.3	−96.6	15.3	14.7	−83.1
$Q_B^{\bullet-}$ (UQ-EM$^{\bullet-}$-ind-SIG)[d]	15.0	14.3	−81.7	17.3	16.6	−93.5
$Q_B^{\bullet-}$ (UQ-EM$^{\bullet-}$-ind-SIG), reopt1[d]	16.2	15.3	−85.5	16.4	15.8	−87.9
UQ-EM$^{\bullet-}$ + (^{i}PrOH)$_6$[d]	15.2	14.6	−84.8	15.8	15.2	−87.1
$A_1^{\bullet-}$ (EMNQ$^{\bullet-}$-nmf-ind)[d]	15.6	14.8	−83.3	17.5	16.8	−86.9
$A_1^{\bullet-}$ (EMNQ$^{\bullet-}$-nmf-ind), reopt3[d]	14.5	13.8	−79.7	17.7	17.0	−87.3
exptl $Q_A^{\bullet-}$ in Zn-bRC$_m$[e]			(−)94			(−)75
exptl $Q_B^{\bullet-}$ in Zn-bRC$_m$[e]			(−)88			(−)82
exptl BQ$^{\bullet-}$ in *i*PrOH[f]			−91.6			−91.6
exptl DQ$^{\bullet-}$ in *i*PrOH[g]			−81.4			−81.4
exptl 2-methyl-NQ in *i*PrOH[h]			(−)78			n.d.
exptl 2-methyl-NQ in PS I[i]	4.5	4.5	(−)77	4.5	4.5	(−)84
calcd $VK_1^{\bullet-}$[j]	13.4	14.0	−83.1	19.6	20.1	−97.3

[a] Cf. Figure 2. Atom labels for A_1 converted in analogy to the numbering used for ubisemiquinone models. [b] Fully optimized gas-phase radical. [c] Isolated radical but with structure taken from the 2/1 1HO-1HN-4HO model. [d] Structures adapted from ref 32; see footnote c of Table 2. [e] Cf. ref 4. [f] From W-band EPR in frozen deteurated 2-propanol.[37] [g] From Q-band EPR in frozen deuterated 2-propanol.[37] [h] Reference 59. [i] Reference 56. [j] B3LYP/EPR-II calculations on an A_1 model made from vitamin K_1 and a methyl-imidazole molecule H-bonded to O_4.[55]

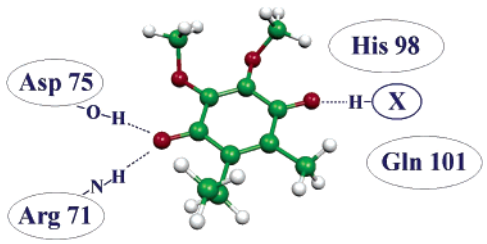

Figure 3. Binding-site model derived for cofactor−protein interactions in the Q_H site of *bo*$_3$ quinol oxidase.

available ESEEM data,[24] with the general model of the binding site by Abramson et al.,[20] and with the *g*-tensor and hyperfine data.[16] On the other hand, we cannot exclude that more hydrogen bonding is present on both sides, in a situation that would be better described by a 3/2 model (see above). Both 2/1 and 3/2 models share an asymmetric yet not single-sided arrangement with one more hydrogen bond to O_1 than to O_4.

4. Conclusions

Our calculations suggest that the hydrogen-bonding environment in the high-affinity (Q_H) binding site of *bo*$_3$ quinol oxidase is asymmetrical to the two carbonyl oxygen atoms O_1 and O_4 of the ubisemiquinone, but not single-sided to O_1 alone. The single-sided model would not be consistent with the rather low g_x component of the *g*-tensor, and it would also give a far too large asymmetry of the two carbonyl ^{13}C hyperfine couplings. Our best models suggest two hydrogen bonds to O_1 and one to O_4, and we have provided a tentative assignment of the protein residues involved, based on the suggested binding site from X-ray crystallography.[20] A 3/2 model with more extensive hydrogen bonding is equally possible. Both of these hydrogen-bond patterns appear to be consistent with the high affinity of the Q_H site for the semiquinone state.

The present quantum chemical calculations of hyperfine and *g*-tensors for a large variety of supermolecular models of ubisemiquinones in different environments have provided appreciable general insight into the interrelationships between hydrogen-bond environment and EPR parameters. While our main goal was to better understand the Q_H binding site of *bo*$_3$ quinol oxidase, the data provided may be used also in other cases, where accurate structural data for the semiquinone state are lacking. While the *g*-tensor is a very compact representation of the spin-density distribution, we may at least rely on the sensitivity of the g_x component for the strength of hydrogen bonding in general and on the larger reduction of g_x by double-sided relative to single-sided hydrogen bonding. The asymmetry of ^{13}C hyperfine couplings of the carbonyl groups reflects the asymmetry of the hydrogen-bonding framework characteristically, if one keeps in mind that one may not straightforwardly transfer HFC values from symmetrical to asymmetrical environments. The ^1H HFCs of the methyl group appear to be difficult to reproduce computationally, as small structural inaccuracies or environmental effects may cause relatively large deviations. Determination of exchangeable proton hyperfine couplings will provide additional useful information, and experiments are currently being performed to determine them.

Acknowledgment. We are grateful to Roman Reviakine for technical support and discussions. This study has been funded by Deutsche Forschungsgemeinschaft (DFG) within the Priority Program SP1051 on "High-Field EPR Spectroscopy in Chemistry, Biology, and Physics" (KA1187/4) and has benefited also from graduate college GRK448 "Moderne Methoden der magnetischen Resonanz in der Materialforschung" at Universität Stuttgart. F.M. acknowledges the DFG Sonderforschungsbereich 472 "Molekulare Bioenergetik" and the Centre for Membrane Proteomics.

Supporting Information Available: Figure S1 shows the variation of Δg_x and Δg_y with the hydrogen-bond distance to O_4 (for 2/1-a 1HO-1HN-4HO model), and Figure S2, the variation of ^{13}C(carbonyl) A_z hyperfine components (C_1 and C_4 positions) with hydrogen-bond distance to O_4 (for 2/1-a 1HO-

1HN-4HO model). Figure S3 provides spin-density isosurface plots and Mulliken atomic spin density values for a number of model complexes. Table S1 gives Cartesian coordinates of three structures modeling possible relative arrangements of 2/1-a 1HO-1HN-4HO model and a double point charge at the heme-a iron position. Table S2 provides structural and EPR parameters for the 2/1-a model where some or all hydrogen bonds have been shortened to 1.60 Å. Table S3 gives Cartesian coordinates of the more specific models of semiquinones in $Q_A^{\bullet-}$, $Q_B^{\bullet-}$, and $A_1^{\bullet-}$ binding sites (cf. also ref 32). Full authorship of ref 42. This material is available free of charge via the Internet at http://pubs.acs.org.

JA053988B